2005-01-2546

Active Vibration Control of Automotive Steering Wheels

Emanuele Bianchini
Vibration-X, S.a.s.

ABSTRACT

Several sources of vibration are felt by a driver of an automobile. Road and engine excitation are the primary sources of vibrations and they are transmitted to the driver by the steering wheel, the floor and the seat. Active vibration control has been a well established method of controlling vibration, but its use has been limited to research laboratories and high end applications. This paper describes an approach of implementing a cost effective active vibration control system applied to a steering column. The active control system has been designed to eliminate the engine idle vibrations being transmitted to the steering wheel. The system is comprised of piezoelectric actuators, sensors and low cost electronics to drive the actuators in an appropriate manner. The first bending mode of the steering column was addressed. The efficacy of the solution was compared to the current production solution (a viscoelastic tuned mass damper tuned for such frequency). A finite element model of the structure was developed and used to size the actuators and locate the sensors. The same model was then used to run simulations of the effects that different control algorithms have on the overall vibration levels of the steering system. A 25 dB reduction at the target mode was achieved numerically. Follow on work will include the implementation of the system into an actual vehicle.

INTRODUCTION

A typical steering system is comprised of a steering wheel and a steering column. These two components are prone to vibration coming from road and engine excitation. The steering column is typically mounted to the frame of the vehicle and has a bolted connection to the frame. It is common practice to eliminate the first mode of vibration by adding a tuned mass damper in series with the steering column so that minimal vibration is transmitted to the steering wheel [1-3]. Such solution is somewhat cumbersome because of its weight and its required customization. One of the critical functions of the steering system is that it has to transfer the static loads from the driver to the wheels, hence leading to a series of conflicting requirements: “hard” (or stiff) for energy transfer and durability, and “soft” (or damped) for comfort. Active vibration control has been explored primarily as a way to introduce variable damping to a suspension system. These systems use piezoelectric or other smart materials in conjunction with a shock absorber. They are typically used as a valve to change the properties of a shock absorber rather than reducing vibrations directly (as a strain type actuator). Another automotive application of smart materials has been in the area of active noise control for automotive passenger cabins. In that case, a very robust multiple input, multiple output control system is required [4, 5]. The application presented here focuses on a simpler, more bounded problem: the control of a single vibration mode. The advantage of this approach is that it leaves the design engineer with the opportunity to design an automotive structure (not necessarily a steering column) that operates above its first natural frequency. Typically this is not common practice, but it has the benefit of making the structure lighter, more tailored to the specific conditions, hence making the overall vehicle more efficient (from weight, fuel and functionality standpoints).

SYSTEM DESIGN

The approach used for this work can be easily transferred to other active vibration control applications. The primary steps included the determination of the problem requirements, the formulation of a finite element model that would represent the system, the control theory model, and the numerical verification that such model would perform as planned.

FE MODELING AND MODEL REDUCTION - A finite element model was received from an automotive manufacturer. Such model was too detailed to be usable in a vibration analysis. It contained 140,000 nodes and 47,000 elements. The majority of the elements were 20-noded brick elements (parabolic solid elements), which are computationally expensive, especially in a full harmonic analysis. The original model is shown in Figure 1. That model was then simplified into a reduced model as shown in Figure 2.

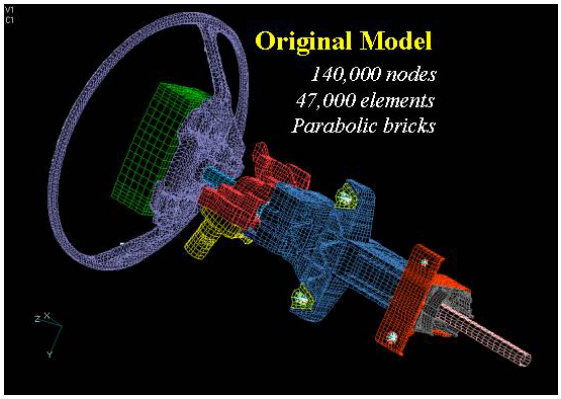

Figure 1: Original FEA model

The reduced model is a very good representation of the more complex model, and it has a much more manageable size (2200 nodes and 2100 linear elements). The reduced model was built in Nastran (FEMAP mesher) and analyzed in Ansys. A typical harmonic response from 10 to 160 Hz at 3 Hz interval solutions was running in just under 2 hours in a PC workstation. The original FEA model would have required a much more powerful computer and a much longer execution time to perform the same run.

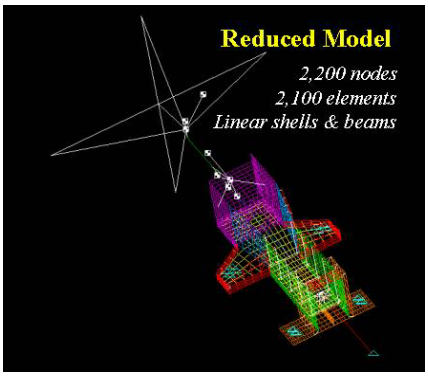

Figure 2: Reduced FEA model

Some of the key features of the reduced model are shown in Figure 3. The main steering wheel and the bracket with the two forward attachment points were modeled by 4-noded shell elements. The rib structure in the channel was modeled by beams with the equivalent cross sectional properties and with the appropriate offset from the mid-plane of the shells. The plastic part used to connect the main casting to the attachment bracket was modeled by rigid elements since its function is to transfer the load from one part to the other. The details of the chamfers, drafts and small features were suppressed since they play a negligible role in the overall dynamic solution. Their inclusion would be computationally extremely expensive. The bolts that are used to connect the steering wheel assembly to the vehicle frame have been replaced by fixed constraints. These nodal constraints are used to input the forcing function simulating the engine idle condition.

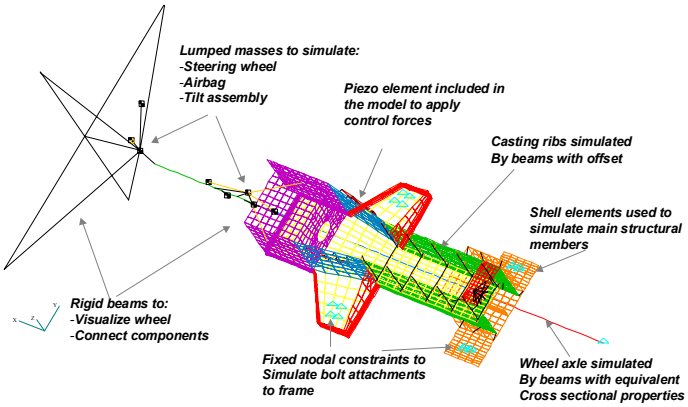

Figure 3: Details of the reduced FEA model

Several assemblies were modeled by their appropriate lumped mass and inertial properties. This approach is extremely helpful in reducing the model size and maintaining accuracy. The proper mass and inertias were found by selecting the appropriate elements in the original finite element. The largest lumped mass was the steering wheel mass and the airbag apparatus attached to it. The tilt assembly and the controls assembly were also modeled by lumped masses. The tilt assembly connects to the steering wheel and the main casting by means of rigid beams with the rotational degree of freedom released for the casting-tilt assembly connection. This condition is most representative of the actual configuration.

Rigid beams were also used to visualize four orthogonal points on the rim of the steering wheel as well. These beams have no effect on the solution. The wheel axle was simulated by beams with equivalent cross sectional property. The forward tip of the wheel axle was constrained in the rotation about its own axis. If this condition would have not been imposed, then the wheel would have been allowed to spin about itself. The universal joint in the upper part of the wheel axle was simulated and connected by rigid beams to the main casting. The finite element model was experimentally validated. The steering column was tested as mounted onto the vehicle. An experimental modal analysis of the system was performed, and although the first few numerical natural frequencies did not exactly match the experimental test, the mode shapes were matched. For example, the first natural frequency of the actual column was about 38 Hz, while the model predicted a 49 Hz frequency. In both cases the mode shape of the first modes matched, so it was decided to continue using the model, and using a frequency shift factor once the implementation will have to take place to make sure that the controller is tuned for the proper frequency.

The piezoelectric actuators were modeled by shell elements offset from the side surface of the main casting. They were connected by rigid elements as shown in Figure 4. The offset allowed the piezo elements to be properly modeled. The size and placement determination is detailed in the next sections.

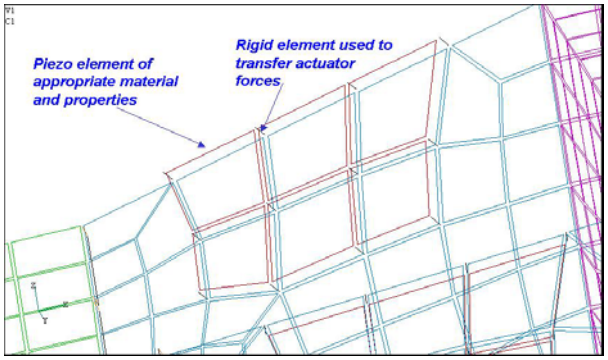

Figure 4: Piezoelectric actuator details

ACTUATOR PLACEMENT AND SIZING – The proper size and placement of the actuators used to control the steering column are optimized for the specific target mode. Since piezoelectric materials are strain-type actuators, the proper location for the piezoelectric actuator is where the modal strains are highest. The size of the actuator depends on the total force required to counter-balance the vibration energy present. There is a trade off between thickness and the surface area of the actuator. Unlike viscoelastic and other damping materials, piezoelectric materials are relatively stiff. Their addition to the baseline structure does change the dynamic properties of the part even without being active or turned "on". An iterative process is typically used, so that the model includes the stiffening effects of the piezoelectric material.

Optimal actuator thickness - The optimal actuator thickness is found by maximizing the induced curvature that the actuator can impart onto the structure. Figure 5 shows a simplified sketch of the cross section where the piezoelectric material is applied. The variables shown in Figure 5 are used in the following analysis.

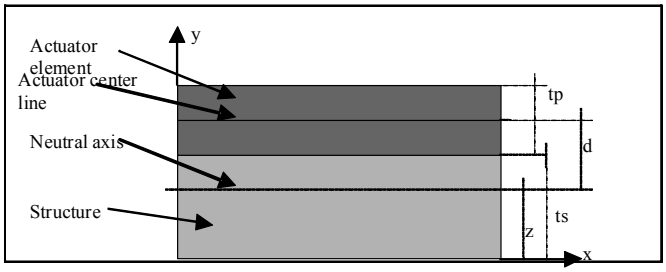

Figure 5: Piezoelectric actuator details

The curvature induced by a piezoelectric actuator can be calculated as:

$$\kappa = \frac{F_p d}{EI} \qquad (1)$$

where κ is the curvature, F_p is the extensional force of the piezo, d is the distance between the center of the actuator and the neutral axis of the structure, and $(EI)_n$ is the combined bending stiffness of the structure. The extensional force per unit edge length that a piezoelectric actuator can exert on a structure can be written as

$$F_p = E_p t_p \Lambda \qquad (2)$$

In this equation, Λ is the free extensional strain of the actuator and E_p is the Young's modulus of the actuator. The moment and force resultants for a generic cross-section are provided in Equation 2. The sign for the moment is chosen such that positive curvature corresponds to compression of the top surface. Also, the moment is dependent on the frame of reference used. For this discussion we chose to place the origin of the frame of reference at the bottom of the plate as shown in Figure 5.

$$\begin{cases} M_r \equiv -\int_A y_r \sigma_x dA \\ F \equiv \int_A \sigma_x dA \end{cases} \qquad (3)$$

Using stress-strain relations for a Bernoulli-Euler beam, the force and moment of Equation 3 can be written as:

$$\begin{aligned} \sigma_x &= E\varepsilon_x \\ \varepsilon_{xr} &= \varepsilon_0 - y_r \kappa \end{aligned} \qquad (4a)$$

$$\begin{cases} M \equiv -\int_A y_r E(\varepsilon_0 - y_r\kappa)dA = \kappa\int_A {y_r}^2 EdA - \varepsilon_0 \int_A y_r EdA \\ F \equiv \int_A E(\varepsilon_0 - y_r\kappa)dA = -\kappa\int_A y_r EdA + \varepsilon_0 \int_A EdA \end{cases} \qquad (4b)$$

Furthermore, defining the zero moment (or extensional stiffness), static moment and second order moment (or bending stiffness) per unit width of the cross section, Equation 4 can be written as:

$$EA \equiv \int Edy \quad (ES)_r \equiv \int y_r Edy \quad (EI)_r \equiv \int {y_r}^2 Edy$$
$$\begin{bmatrix} M \\ F \end{bmatrix}_r = \begin{bmatrix} (EI)_r & -(ES)_r \\ -(ES)_r & EA \end{bmatrix} \begin{bmatrix} \kappa \\ \varepsilon_0 \end{bmatrix} \qquad (5)$$

The index r indicates that the terms are calculated with respect to a frame of reference r. If we translate the origin by a distance z so that $y_z = y - z$, we can use the definitions of the resultants (Equation 3) and of curvature and strain to be:

$$\begin{cases} M_z \equiv -\int_A y_z \sigma_x dA = -\int_A (y_r - z)\sigma_x dA = -\int_A y_r \sigma_x dA + z\int_A \sigma_x dA = M_r + zF_r \\ F_z \equiv \int_A \sigma_x dA = F_r \end{cases}$$
$$\begin{bmatrix} M \\ F \end{bmatrix}_z = \begin{bmatrix} 1 & z \\ 0 & 1 \end{bmatrix} \begin{bmatrix} M \\ F \end{bmatrix}_r = T \begin{bmatrix} M \\ F \end{bmatrix}_r$$
$$\varepsilon_{0z} = \varepsilon_{0r} - z\kappa$$
$$\begin{bmatrix} \kappa \\ \varepsilon_0 \end{bmatrix}_z = \begin{bmatrix} 1 & 0 \\ -z & 1 \end{bmatrix} \begin{bmatrix} \kappa \\ \varepsilon_0 \end{bmatrix}_r \Rightarrow \begin{bmatrix} \kappa \\ \varepsilon_0 \end{bmatrix}_r = T^{-1} \begin{bmatrix} \kappa \\ \varepsilon_0 \end{bmatrix}_z \qquad (6)$$

The force resultants and deformations are related in the translated coordinate system by

$$\begin{bmatrix} M \\ F \end{bmatrix}_z = T\begin{bmatrix} M \\ F \end{bmatrix}_r = T\begin{bmatrix} EI & -ES \\ -ES & EA \end{bmatrix}\begin{bmatrix} \kappa \\ \varepsilon_0 \end{bmatrix}_r = T\begin{bmatrix} EI & -ES \\ -ES & EA \end{bmatrix}T^{-1}\begin{bmatrix} \kappa \\ \varepsilon_0 \end{bmatrix}_z$$
$$= \begin{bmatrix} (EI)_r - 2z(ES)_r + z^2EA & -(ES)_r + zEA \\ -(ES)_r + zEA & EA \end{bmatrix}\begin{bmatrix} \kappa \\ \varepsilon_0 \end{bmatrix}_z = \begin{bmatrix} (EI)_z & -(ES)_z \\ -(ES)_z & EA \end{bmatrix}\begin{bmatrix} \kappa \\ \varepsilon_0 \end{bmatrix}_z \quad (7)$$

The neutral axis of a structure is defined as the axis along which the bending and extension equations of a structure are uncoupled. In other words, to find the neutral axis of a structure, the static moment $(ES)_z$ must be zero. From Equation 7, we can derive that, for z=n with n being the distance to the neutral axis

$$(ES)_z = -(ES)_r + nEA = 0$$
$$n = (EA)^{-1}(ES)_r \quad (8)$$

which gives the location of the neutral axis. From the above equation, we can derive the distance from the neutral axis to the piezo center line to be

$$d = \left(t_s + \frac{t_p}{2} - n\right) \quad (9)$$

Substituting this value into equation 1, we can express the induced curvature as a ratio of polynomial functions in tp. Note that $(ES)_z$, (EA) and $(EI)_n$ are analytical integrals of polynomials containing E_p , t_p and t_s.as well as the Young's modulus of the structure, E_s , and the width of the structure w.

$$\kappa = \frac{E_p t_p \Lambda d}{(EI)_n} = E_p t_p \Lambda \frac{f(tp)}{g(tp)} \quad (10)$$

An example of the above function is given in Figure 6. Since the numerator is a second order polynomial in tp and the denominator a third order polynomial in tp, there is a local maximum of the curvature for the optimal actuator thickness.

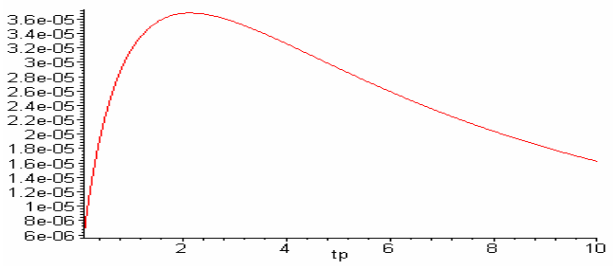

Figure 6: Induced curvature as a function of piezo thickness

For the case of the steering wheel in consideration, the modulus of the piezoelectric material (Ep) was assumed to be 60 GPa, the modulus of the structure (Es) was 45 GPa, and the thickness of the structure (ts) was 5.5 mm. Using the above method, the optimum piezo actuator thickness (tp_{opt}) was derived to be 2.2 mm.

Optimal actuator location – Since piezoelectric materials are used as strain-based actuators, the best actuator location for each mode of vibration is the one that exhibits the highest localized strain at the particular frequency of interest. Therefore, knowing the strain mode shapes for the modes to be controlled is key to an effective control solution.

To a first approximation, the authority of an actuator over a given mode is proportional to the difference in rotation between opposite edges. This occurs over areas where there is the highest strain (being the spatial derivative of rotation, or the places where there are the greatest gradients of rotation). Figure 7 shows the areas of high strain in the model.

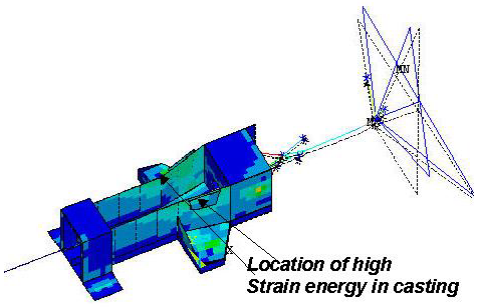

Figure 7: Location of high strain energy for the first mode

For multiple modes, a trade-off study between the modes of interest will have to be made, since the optimum actuator location will vary with the mode. Different optimization schemes can be used to determine such locations. In general, it is best to locate piezoelectric actuators away from strain node lines. A strain node line is defined as the location where the strain changes sign (from positive to negative or vice versa). If such condition exists, then the actuator will become quite ineffective since one section of the actuator will actuate in one direction and the other in the opposite direction, canceling their efficiency.

Once the location and thickness of actuators is determined, the last variable is the total area and number of actuators to be used. The upper limit is set by the amount of current needed to drive the actuators and by the extent of the high strain areas to avoid crossing strain node lines with the actuator. The lower limit is set by the minimum acceptable performance of the system.

The sensor location and type is an important consideration for a vibration control system. In this numerical case, the sensor location was the performance point. In the case of an actual system, an accelerometer or a strain gauge may be used.

DYNAMIC ANALYSIS - At first a series of modal analysis runs were made to find the location of the highest strain energy. This location would then be used to apply the piezoelectric elements that are used as actuators. Once the location of the actuators was found, then the plate elements were added as previously shown in Figure 4.

Two harmonic analyses were run. At first a full harmonic analysis was run using the input disturbance at the four frame attachment points. The disturbance to performance transfer function was obtained. Then a second harmonic solution using the actuator input from the actuator was performed. The actuator to performance transfer function was obtained. These two functions were used in the control design described in the next section.

CONTROL DESIGN

For the control design of the system, a feedback approach with Positive Position Feedback (PPF) solution approach was selected. This approach will be briefly discussed in the following paragraphs, along with the results and the control algorithms.

FEEDBACK CONTROL - Feedback control uses a signal measured on the system and feeds it to a compensator K. The compensator contains a transfer function detailing how to react to a certain input, and sends a control signal to the actuators. The actuators react to the control signal and counteract the movement in the structure. A diagram of this kind of system is presented in Figure 8.

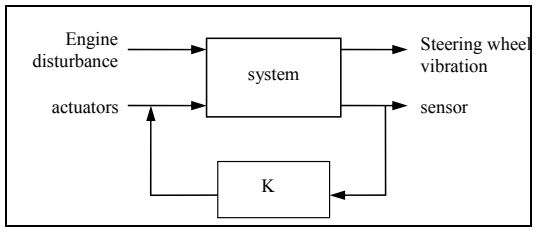

Figure 8: Feedback control loop

In this case, the performance metric is the steering wheel vibration recorded at the center of gravity of the wheel. This signal is computed and used to determine the control function to be implemented in the compensator K. The signal fed back is a displacement result obtained at the CG of the wheel. Not as much in a numerical simulation as this one, but in a real system, the placement and size of these sensors is important to get a clean and co-located function to control. “Clean” means that the signal to noise ratio is large, while “co-located” means that the transfer function from actuator to sensor has a pattern of alternating poles and zeros. This criterion is important for control design purposes and is in general obtained by placing the sensors as close as possible to the actuators.

SINGLE MODE CONTROL DESIGN - For a single-mode harmonic disturbance, active damping was achieved using a positive position feedback or PPF. A compensator containing a complex conjugate pair of poles coinciding with the natural frequency of the target mode is used. The general expression for this kind of compensator is:

$$K = \frac{k}{s^2 + 2\zeta\omega_p s + \omega_p{}^2} \qquad (11)$$

Once the control approach is defined, the system has to be characterized by measuring the system transfer functions. The relationship between the two inputs, control and disturbance, and the two outputs, sensor and performance, are required. In this case, the sensor and the performance are the same. The Ansys finite element model described in the previous section was used to represent the system. A sine swept harmonic forcing function was input to the model. The source of excitation was the attachment to the rest of the car frame (by the four bolted connections of the steering column casting). The response at the actuator location and at the sensor location was recorded. Secondly, the actuators were driven by the same swept sine harmonic function, and the response was recorded at the sensor location (which is also the performance point). The signals can then be divided over each other, and analyzed in frequency domain using an FFT algorithm. The resulting transfer functions are shown in Figure 9 and Figure 10.

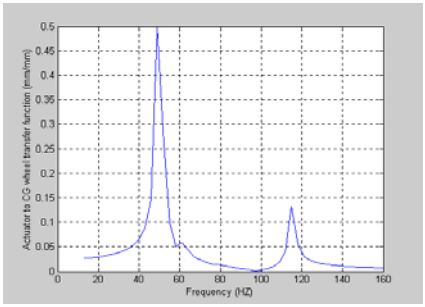

Figure 9: Actuator to performance transfer function

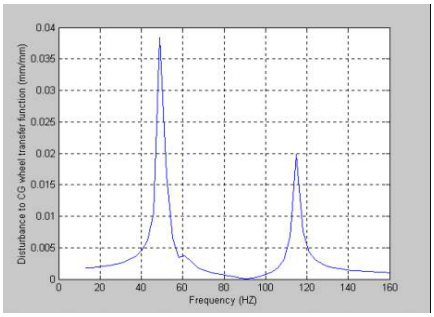

Figure 10: Disturbance to performance transfer function

The transfer functions shown in Figures 9 and 10 are then transferred to a state-space representation so that they can be easily used and manipulated in the control software. The system shown in Figure 8 is now ready to be analyzed numerically. The goal of the model is to change the values of the compensator so that the vibration at the sensor location (also performance location) is minimized. The values of the controller coefficients can be changed to optimize the overall response of the system. Poles and zeros were added to the compensator until the proper balance between stability and vibration reduction could be obtained. Control gains were also adjusted so that the vibration reduction at the target frequency could be obtained without making the system unstable at other frequencies.

The optimal control law for this system, under the restrictions described above, is shown in Figure 11.

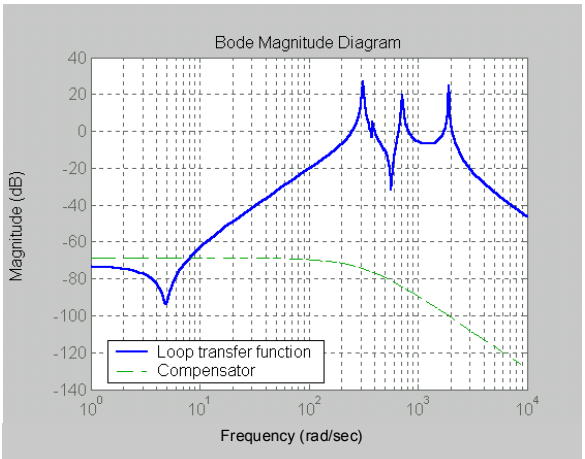

Figure 11: Transfer function from disturbance to performance

Figure 11 shows the loop gain resulting from the control law above. The loop transfer function represents the amount of effort (forces) put into the system at any given frequency. Notice that at all of the frequencies at which the loop transfer function exceeds zero, the control adds "control forces" to the system. In this case, it happens in the first three modes of vibration in the frequency range considered.

RESULTS SUMMARY

The best way to view the performance of a broadband control system is to view its frequency response without the control loop connected (open loop) and compare it to the same response with the control loop on (closed loop performance). We can compare the open and closed loop performances in the Matlab-based simulation. The difference between open and closed loop response is given in Figure 12.

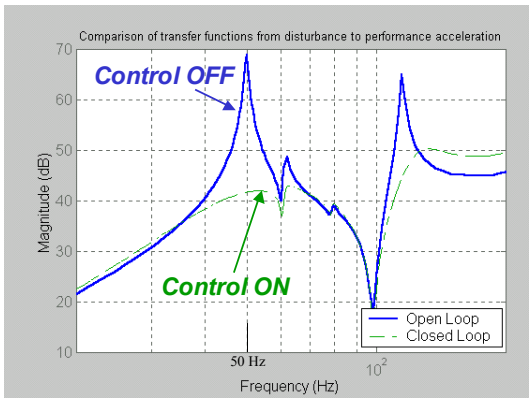

Figure 12: Modeled open and closed loop performance

Notice from Figure 12 that the first natural frequency of the model (50Hz) is completely eliminated and a reduction of almost 30dB is obtained. Additionally, the second bending mode is reduced by over 10 dB due to the spill over effects of the control system.

In order to further explore the effectiveness of the active control used, two time domain simulations were run using Simulink (a software extension of Matlab). The block diagram used is shown in Figure 8. Figure 13 shows the system response at the steering wheel's CG due to a sine wave disturbance tuned for the first bending mode at 49Hz. Notice that the active control response has a much reduced acceleration response (over 20 times reduction from 4.5m/s^2 to 0.2 m/s^2).

Figure 14 shows the response of the system with and without control if a random chirp is used as input. The top plot shows the input signal, and the bottom plot shows the effectiveness of the active control, which eliminates the entire chirp. The total weight of the actuators used for all three simulations was not much more than 50 grams. The design can be modified to add or subtract additional actuators. In the next phase of the program Vibration-X will instrument an actual steering column with sensors, actuators and electronics and validate the numerical results described herein.

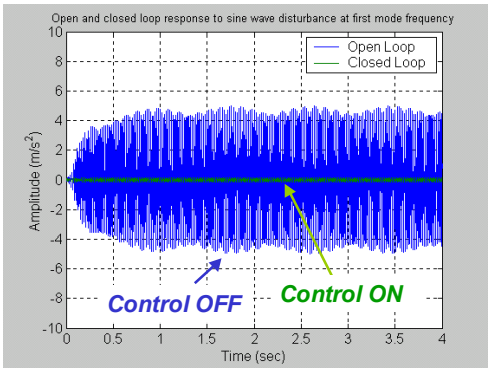

Figure 13: Open and Closed Loop performance to a sine wave disturbance at the first mode frequency

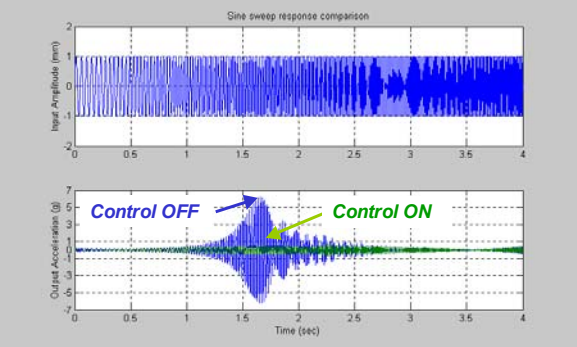

Figure 14: Open and closed loop performance to a random chirp simulation

CONCLUSION

The current paper describes the numerical work performed in reducing vibration in a steering column by using active vibration control. A 25 dB vibration reduction was numerically demonstrated using a limited weight increase of the system. These results need to be experimentally validated to provide a more complete demonstration of feasibility of the active vibration control system. Actuators and sensors have been built and integrated into an automotive steering column. Figure 15 shows a piezoelectric sensor that has been produced by Vibration-X for this task. The actuator is currently under development, but it will resemble the piezoelectric sensor shown in Figure 15 but in a larger footprint.

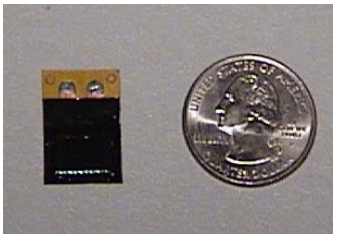

Figure 15: Sample piezoelectric sensor

Electronics have been built and will resemble these shown in Figure 16. A switching amplifier is used in this application so that the piezoelectric actuators can deliver the force required. For this application, a voltage supplied by a typical automotive power supply (12-14 Volts) can be stepped up by the switching amplifier so that it delivers +/- 250 Volts to the piezoelectric actuator. This type of voltage is typically required by the actuator to effectively reduce the vibration of the steering column. The switching amplifier is more efficient than a conventional linear amplifier, but it has the drawback that it does generate noise as it switches from the high voltage rail to the low voltage rail. For this reason, the amplifier should be enclosed with a cover so that its noise level is reduced. These levels are typically below automotive noise levels, but they should still be considered in the design of the solution.

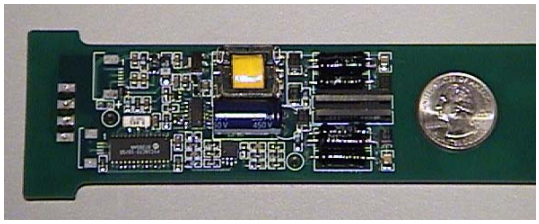

Figure 16: Sample drive electronics

The approach described in this paper can be used in the future for similar implementations of active vibration control applied to automotive parts and components. Although the cost of the implementation and the cost of the final solution it is higher than a conventional passive solution, the weight savings and the reduction achieved may warrant the expense. As a final note, such a system described here can be manufactured for few tens of dollars in medium to high automotive quantities.

ACKNOWLEDGMENTS

The author would like to acknowledge Marco Giovanardi for his work and input on the control design simulation.

REFERENCES

1. Black, M.D., and Rao, M.D., “Evaluation and reduction of steering column vibration of a rear wheel drive sedan,” *Int. J. Vehicle Noise and Vibration*, Vol. 1, No. 1 2, 2004.
2. Bolz, J, et al., “Optimization of Power Steering System Vibration in Passenger Cars,” Society of Automotive Engineers, SAE 951253, 1995.
3. Sahinkaya, Y., et al., “A Novel Steering Vibration Stabilizer,” Society of Automotive Engineers, SAE 960930, 1996.
4. Kowalczyk, K., Svaricek, F., Bohn, C. and Kakosch, H.J., “Active Control of Engine-Induced Vibrations: An Experimental Comparison of the FxLMS-and the Disturbance Observer Approach,” Proceedings of the Actuator 2004 Conference, Bremen, Germany, June 2004.
5. Meschke, J., Kindermann, L., Schmidt, K., and Thormann, V., “Vehicle Improvements by use of Active Vibro-Acoustic Systems,” Proceedings of the Actuator 2004 Conference, Bremen, Germany, June 2004.

CONTACT

Emanuele Bianchini is the president of Vibration-X, S.a.s., a small company with the primary focus of implementing smart structure solutions to future products. Mr. Bianchini can be contacted at exb@vibration-x.com or at emanuele@vibration-x.it.